Interleaved Soft-Switching Boost Converter for Photovoltaic Power-Generation System

AUTHOR: Ms.N.ABIRAMI ,Assistant Professor, Electrical and Electronics Engineering, V.S.B Engineering College,Karur

Co-authors: R.dhivya, S.gunavathi, S.janani,V.Raagavi, Electrical and Electronics ,VSB Engineering College,Karur

***Abstract*—In this paper, a interleaved soft switching boost converter (ISSBC) for a photovoltaic (PV) power-generation system is proposed. The topology used raises the efficiency for the dc/dc converter of the PV power conditioning system (PVPCS), and it minimizes switching losses by adopting a resonant soft-switching method. A detailed mode analysis of the proposed topology is pre-sented. The feasibility of the proposed topology is experimentally verified for a 1.2-kW prototype. The experimental results imply that 97.28% efficiency is achieved under the full-load condition. Consequently, it is confirmed that the overall efficiency is increased by about 1.5% compared with the conventional hard switching in-terleaved boost converter.**

***Index Terms*—Boost converter, interleaved, maximum power-point tracking (MPPT), photovoltaic (PV) power-generation systems, resonant converter, soft-switching.**

I. INTRODUCTION

ECENTLY, photovoltaic (PV) energy has attracted interest **R**as a next generation energy source capable of solving the problems of global warming and energy exhaustion caused by increasing energy consumption. PV energy avoids unnecessary fuel expenses and there is no air pollution or waste. Also, there are no mechanical vibrations or noises because the components of power generation based on PV energy use semiconductors. The life cycle of the solar cell is more than 20 years, and it can minimize maintenance and management expenses.

The output power of the solar cell is easily changed by the surrounding conditions such as irradiation and temperature, and also its efficiency is low. Thus high efficiency is required for the power conditioning system (PCS), which transmits power from the PV array to the load. In general, a single-phase PV PCS consists of two conversion stages (i.e., dc/dc conversion stage and dc/ac conversion stage). The dc/dc converter is the first stage and it performs maximum power-point tracking (MPPT) and guarantees the dc-link voltage under low irradiance conditions [1], [2].

This paper proposes a high efficiency dc/dc boost converter to increase the overall efficiency of PV power conditioning system (PVPCS) [3]–[8]. We studied a 2-phase interleaved boost con-verter integrated with a single-switch type soft-switching boost converter. The proposed single-switch type soft-switching boost converter can minimize switching loss by adopting a resonant soft-switching method. And, no additional switches are needed for soft switching [9]–[15].

However, the drawback of this converter is that the volt-age across the switch is very high during the resonance mode. The voltage across the switch depends on the parameters of the resonant components (i.e., resonant inductance and resonant capacitance) and the resonant inductor current. In this paper, the optimal design of the resonant components and the inter-leaved method is applied for resonant current reduction. Since the interleaved method distributes the input current according to each phase, it can decrease the current rating of the switch-ing device. Also, it can reduce the input current ripple, output voltage ripple, and size of the passive components [16]–[18]. The proposed soft-switching interleaved boost converter can not only exploit the interleaved converter but also reduce switching losses through the soft-switching technique. Therefore, the out-put power of the PV array can be boosted with high efficiency.

This paper presents the operational principle of the converter, a theoretical analysis and design guidelines. A 1.2-kW prototype of the converter has been built, and simulation and experimental results are provided to verify the theoretical analysis.

II. PROPOSED TOPOLOGY

A. Proposed Soft-Switching Boost Converter

The interleaved boost converter consists of two single-phase boost converters connected in parallel. The two PWM signal difference is 180° when each switch is controlled with the in-terleaving method.

Because each inductor current magnitude is decreased ac-cording to one per phase, we can reduce the inductor size and inductance when the input current flows through two boost in-ductors. The input current ripple is decreased because the input current is the sum of each current of inductor L_1 and L_2 .

Fig. 1(a) shows the proposed single-switch type soft-switching boost converter [19]. One resonant inductor, two ca-pacitors, and two diodes are added to a conventional boost con-verter for soft switching using resonance. Fig. 1(b) shows the interleaved soft-switching boost converter (ISSBC) proposed in this paper. Two single-phase soft-switching boost converters are connected in parallel and then to a single output capacitor.

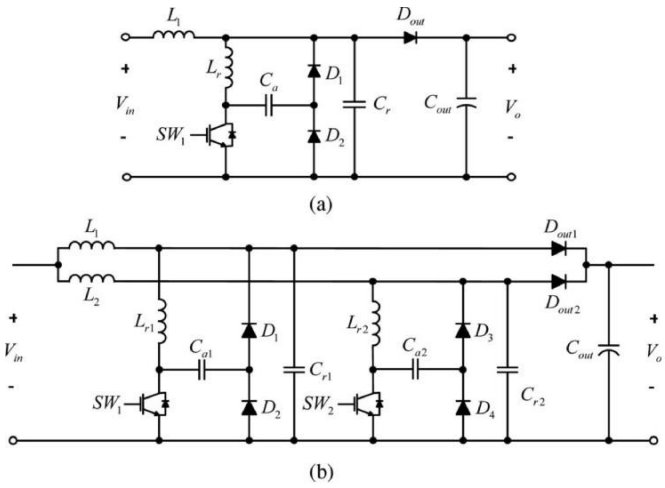

Fig. 1. Proposed soft-switching boost converter. (a) Proposed single-switch soft-switching boost converter. (b) ISSBC

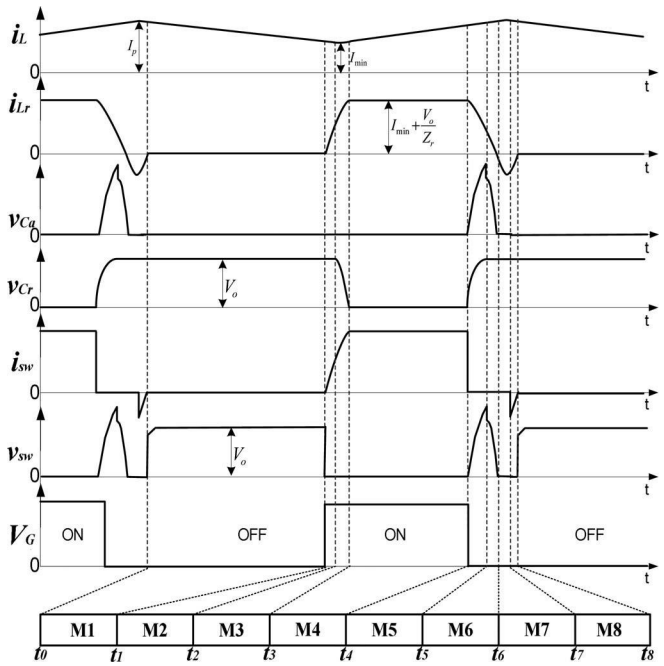

Fig. 2. Key waveforms of proposed converter.

B. Mode Analysis of the Proposed Converter

Each mode is presented during one switching cycle of steady-state operation of the proposed converter.

For illustrating the soft-switching operation using resonance, we describe the operation modes of a single-phase soft-switching boost converter [see Fig. 1(a)], which consists of the proposed ISSBC.

The key waveforms associated with the operation stages are shown in Fig. 2. There are operation modes shown in Fig. 3, and the duty ratio is assumed to be 0.5 in order to simplify the analysis. The operation can be analyzed in terms of eight modes according to the operating conditions defined in the following paragraphs.

1) All switching devices and passive elements are ideal.

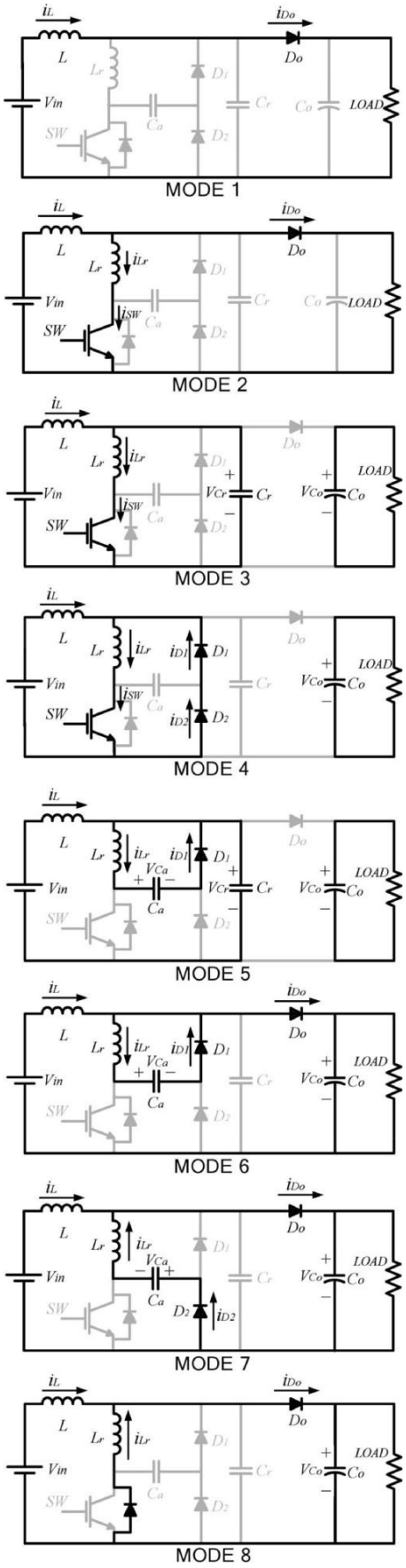

Fig. 3. Operational modes of proposed converter.

2) The parasitic components of all switching devices and elements are ignored.
3) It is assumed that the initial value of each operation mode is equal to zero.

Mode 1 ($t_0 \le t < t_1$): The switch is in the off state and the dc output of the solar cell array is transmitted directly to the load through L and D_{out} . In this mode, the main inductor voltage becomes $-(V_o - V_{in})$. Thus, the main inductor current decreases linearly

$$i_L(t) = i_L(t_0) - \frac{V_o - V_{in}}{L} t \quad (1)$$

$$i_{Lr}(t) = 0, \quad v_{Cr}(t) = V_o, \quad v_{Ca}(t) = 0 \quad (2)$$

$$i_L(t_1) = I_1. \quad (3)$$

Mode 2 ($t_1 \le t < t_2$): In mode 2, the switch is turned on under zero-current switching (ZCS) because of the resonant inductor L_r . In this case, as the output voltage is supplied to the resonant inductor L_r , the current increases linearly. When the resonant current i_{Lr} becomes equal to the main inductor current i_L , the current of the output side diode D_{out} becomes zero

$$i_L(t) = I_1 - \frac{V_o - V_{in}}{L} t \quad (4)$$

$$i_{Lr}(t) = \frac{V_o}{L_r} t, \quad v_{Cr}(t) = V_o, \quad v_{Ca}(t) = 0 \quad (5)$$

$$i_L(t_2) \approx I_{min}, \quad i_{Lr}(t_2) \approx I_{min}. \quad (6)$$

Mode 3 ($t_2 \le t < t_3$): When the output current i_{Dout} becomes zero, the mode starts. In this mode, the resonant inductor L_r and the resonant capacitor C_r resonate and the voltage of C_r decreases from the output voltage V_o to zero. In this case, the main inductor current i_L flows through L_r and the switch

$$i_L(t) \approx I_{min}, \quad v_{Ca}(t) = 0 \quad (7)$$

$$i_{Lr}(t) = I_{min} + \frac{V_o}{Z_r} \sin \omega_r t \quad (8)$$

$$v_{Cr}(t) = V_o \cos \omega_r t \quad (9)$$

$$i_{Lr}(t_3) = I_2, \quad v_{Cr}(t_3) = 0 \quad (10)$$

$$\omega_r = 1/\sqrt{L_r C_r}, \quad Z_r = \sqrt{L_r/C_r} \quad (11)$$

Mode 4 ($t_3 \le t < t_4$): When the resonant capacitor voltage V_{Cr} becomes zero, the two auxiliary diodes D_1 and D_2 are turned on and the mode starts. In this mode, the resonant inductor current is separated into two parts. One is the main inductor current i_L and the other is the current turning through the two auxiliary diodes. The main inductor current i_L increases linearly

$$i_L(t) = I_{min} + \frac{V_{in}}{L} t \quad (12)$$

$$i_{Lr}(t) \approx I_2 \quad (13)$$

$$v_{Cr}(t) = 0, \quad v_{Ca}(t) = 0 \quad (14)$$

$$i_L(t_4) = I_3, \quad i_{Lr}(t_4) = I_2. \quad (15)$$

Mode 5 ($t_4 \le t < t_5$): In mode 5, the switch turns off under the zero-voltage condition because of the auxiliary resonant capacitor C_a . There are two current loops. One is the L-C_r - V_i n loop for which the voltage of the resonant capacitor C_r increases linearly from zero to the output voltage V_o . The other is the L_r –C_a –D_1 loop for which the second resonance occurs. The energy stored in L_r is transferred to C_a . The resonant current i_{Lr} decreases linearly and the voltage across C_a becomes maximal

$$i_L(t) \approx I_3 = I_{max} \quad (16)$$

$$i_{Lr}(t) = I_2 \cos \omega_a t \quad (17)$$

$$v_{Ca}(t) = Z_r I_2 \sin \omega_a t, \quad v_{Cr}(t) = I_3/C_a \quad (18)$$

$$\omega_a = 1/\sqrt{L_r C_a} \quad (19)$$

$$Z_a = \sqrt{L_r/C_a}. \quad (20)$$

Mode 6 ($t_5 \le t < t_6$): When the resonant capacitor voltage v_{Cr} is equal to the output voltage V_o , the mode starts. In this mode, the energy flow from L_r to C_a is completed and the resonant current i_{Lr} becomes zero

$$i_L(t) = I_3 - \frac{V_o - V_{in}}{L} t \quad (21)$$

$$i_{Lr}(t) = I_2 \cos \omega_a t \quad (22)$$

$$v_{Ca}(t) = Z_r I_2 \sin \omega_a t, \quad v_{Cr}(t) = V_o \quad (23)$$

$$v_{Ca}(t_6) = Z_a I_3. \quad (24)$$

Mode 7 ($t_6 \le t < t_7$): In mode 7, the voltage of C_a decreases, continuously resonates on the D_2 –C_a –L_r –D_{out} –C_o loop and the energy is transferred from C_a to L_r . When the C_a voltage becomes zero, the resonant current i_{Lr} is the reverse of the cur-rent direction of mode 6. When the voltage of C_a becomes zero, the antiparallel diode of the switch turns on and it transitions to the next mode

$$i_L(t) = I_3 - \frac{V_o - V_{in}}{L} t, \quad i_{Lr}(t_6) = I_4 \quad (25)$$

$$i_{Lr}(t) = \frac{V_o}{Z_a} - I_2 \sin \omega_a t, \quad i_{Lr}(t) = I_5 \quad (26)$$

$$v_{Cr}(t) = V_o \quad (27)$$

$$v_{Ca}(t) = V_o - (V_o - Z_a I_2) \cos \omega_a t = V_2. \quad (28)$$

Mode 8 ($t_7 \le t < t_8$): There are two current loops. The main inductor current i_L transmits energy to the output through D_{out} and decreases linearly. The resonant inductor current i_{Lr} also transmits energy to the load through D_{out} and flows through the antiparallel diode of the switch. When the resonant inductor current i_{Lr} becomes zero, mode 8 ends

$$i_L(t) = I_4 + \frac{V_o - V_{in}}{L} t, \quad i_{Lr}(t_8) = I_6 \quad (29)$$

$$i_{Lr}(t) = I_5 \sqrt{\frac{C_a}{L_r}} t, \quad i_{Lr}(t_8) = 0 \quad (30)$$

$$v_{Cr}(t) = V_o \quad (31)$$

$$v_{Ca}(t) = 0. \quad (32)$$

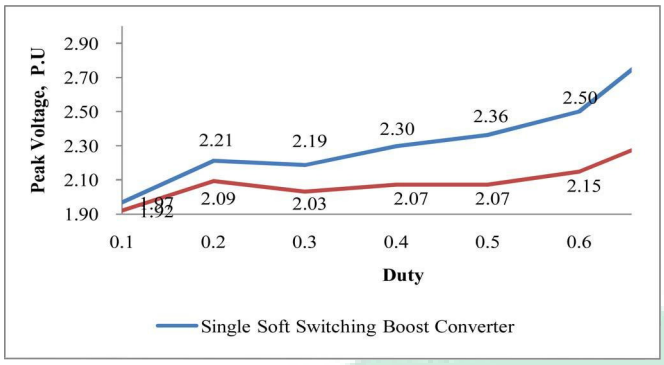

Fig. 4. Comparison of the peak voltage of switching devices between SSSBC and ISSBC (1 p.u. = output voltage).

TABLE I
EXPERIMENTAL PARAMETERS

Parameter	Symbol	Value	Unit
Input voltage	V_{in}	200-350	V
Output voltage	V_o	400	V
Rated power	P_o	1.2	kW
Main inductor	L_1, L_2	1	mH
Resonant inductor	L_{r1}, L_{r2}	50.6	μH
Resonant capacitor	C_{r1}, C_{r2}	100	nF
Auxiliary capacitor	C_{a1}, C_{a2}	10	nF
Output capacitor	C_{out}	10	μF
Switching frequency	f_{sw}	30	kHz

III. DESIGN PROCEDURES OF THE PROPOSED CONVERTER

A. Switch Peak Voltage Analysis and Parameter Design

In mode 5, the current that flows through the L_r–C_a–D_1 loop should be large enough for resonance. As described by (18), the voltage across the auxiliary resonant capacitor C_a is as high as I_2 during this resonant period.

$$v_{SW}(t) = v_{Ca}(t) + v_{Cr}(t) \tag{33}$$

The amplitude of the switch voltage is determined by the res-onant devices and the resonant current. To minimize the peak voltage of the switch, designs for optimal parameters of resonant components are included and the interleaved method is adopted. Because the interleaved method distributes the input current ac-cording to each phase, it can decrease the current rating of the switching device. Thus, it can reduce the peak voltage across the switch, input current ripple, output voltage ripple and size of passive components.

Fig. 4 depicts the peak voltage across the switch of the Single Soft-switching Boost Converter (SSSBC) and ISSBC according to the duty ratio under a full load. The peak voltage of switch is represented in p.u. (per unit), and 1 p.u. is signified the 400 V of output voltage in this paper. The ISSBC reduces the peak voltage across the switch by about 10–20% compared with the SSSBC.

B. Selection of Resonant Inductor and Capacitor

The ZVS condition of the switch is affected by the auxiliary resonant capacitor C_a. In mode 5, the current that flows through the L_r–C_a–D_1 loop should be large enough for resonance. In general, the snubber capacitance has to be more than ten times the parasitic capacitance. The resonant capacitance C_a has to be more than 20 times the output capacitance of the switch, because the C_a is charged by the resonant inductor current (it is about 2 times the main inductor current) during the switch turn-off period, represented as follows:

$$C_a > 20C_{oes}. \tag{34}$$

In mode 3, the resonant inductor current is represented by (8). The period of resonance between resonant inductance L_r and resonant capacitance C_r is about a quarter of the entire resonant period. In general, the rising time of the resonant inductor current is 10% of the minimum on-time of the switch. However, for satisfaction of the ZVS condition, the rising time of the resonant inductor current is 50% of the minimum on-time in this paper, as represented by

$$t_3 - t_1 = \frac{L_r}{V_o} I_{min} + \frac{T_r}{4} < 0.5 D_{min} T \tag{35}$$

where $T_r = 1/f_s = 2\pi\sqrt{L_r C_r}$, $T = 1/f_{SW}$, and $D_{min} = (V_o - V_{in\,min})/V_o$.

From (18) and (35), the resonant capacitance C_r can be de-fined as

$$C_r > \frac{D_{min}^2}{\pi^2 L_r f_{SW}^2} + \frac{I_{min}^2 L_r}{\pi^2 V_o^2} - \frac{2I_{min} D_{min}}{\pi^2 V_o f_{SW}^2}. \tag{36}$$

Since $(2I_{min} D_{min})/(\pi^2 V_o f_{SW}^2) \approx 0$ in (36), this equation can be rewritten as follows:

$$C_r > \frac{D_{min}^2}{\pi^2 L_r f_{SW}^2} + \frac{I_{min}^2 L_r}{\pi^2 V_o^2} \tag{37}$$

$$L_r = \{V_o/(I_2 - I_{min})\}^2 C_r \tag{38}$$

where $I_2 - I_{min} = V_o/Z_r = V_o C_r/\sqrt{L_r}$.

From (37) and (38), C_r can be defined as

$$C_r > \frac{D_{min}(I_2 - I_{min})}{\pi^2 V_o f_{SW}^2} \sqrt{1 - I_{min}^2/\pi^2 (I_2 - I_{min})^2}. \tag{39}$$

From (38), the resonant inductor parameter is expressed as

$$L_r < (2 \times 0.85 \frac{C_s}{} - 1) V_o \left(\frac{I_p}{\pi C_s}\right)^2 \tag{40}$$

where $C_s = C_r C_a/(C_r + C_a)$, $V_o - V_2 \approx 0.85 V_o$.

C. Design Example

In this section, the design procedure of the proposed con-verter is based on the derived equations. Table I shows the design parameters of the proposed boost converter. And, the design guidelines herein provide a proper tool to help choose resonant components and ensure the appropriate operation of the resonance converter.

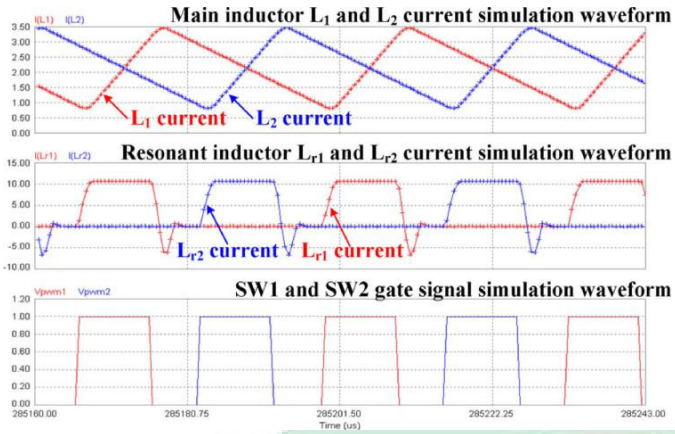

Fig. 5. Simulation result of current of L_1 , L_2 , $L_{r\,1}$, $L_{r\,2}$, and switching signals.

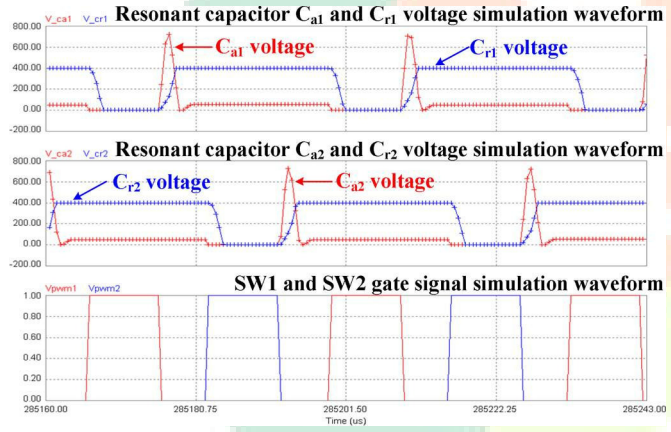

Fig. 6. Simulation result of voltage of $C_{r\,1}$, $C_{a\,1}$, $C_{r\,2}$, $C_{a\,2}$, and switching signals.

IV. SIMULATION

The Powersim simulation software was used to analyze the operational characteristics of the proposed soft-switching inter-leaved boost converter. The design parameters for the simulation are shown in Table I.

Fig. 5 shows the current waveforms of the main inductor and resonant inductor, and the gate signals (SW1 and SW2) of the proposed soft-switching interleaved boost converter. The main inductor currents ($i_{L\,1}$ and $i_{L\,1}$) increase and decrease linearly according to the gate signals. The phase difference of each waveform is 180°.

Also, the resonant inductors store and release energy accord-ing to the gate signals. Fig. 6 shows the voltage waveforms of the resonant capacitor and auxiliary resonant capacitor, and gate signals (SW1 and SW2). The peak voltage of $V_{C\,a}$ is higher than that of the resonant capacitor voltage $V_{C\,r}$.

When the switch turns off, the auxiliary resonant capacitor voltage $V_{C\,a}$ increases and then decreases to the zero level, sat-isfying the ZVS condition represented by (36).

Fig. 7 shows the voltage and current waveforms of the switches and gate signals. The switches SW1 and SW2 are turned on under ZCS and turned off under ZVS.

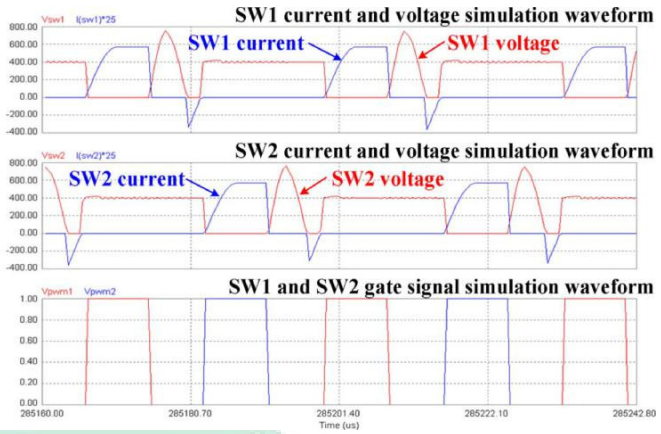

Fig. 7. Simulation result of main switch current, voltage, and gate signals.

TABLE II
PARAMETERS OF SWITCH AND DIODE

Part Number	Symbol	Value	Unit
FGA25N120FTD (IGBT)	I_C (100°C)	25	A
	$V_{CE(sat)}$	1.6	V
	V_{CES}	1200	V
	C_{oes}	130	pF
80EPF06 (Fast soft recovery)	I_F (95°C)	80	A
	V_F	1.25	V
	V_{RRM}	600	V
	t_{rr}	70	ns

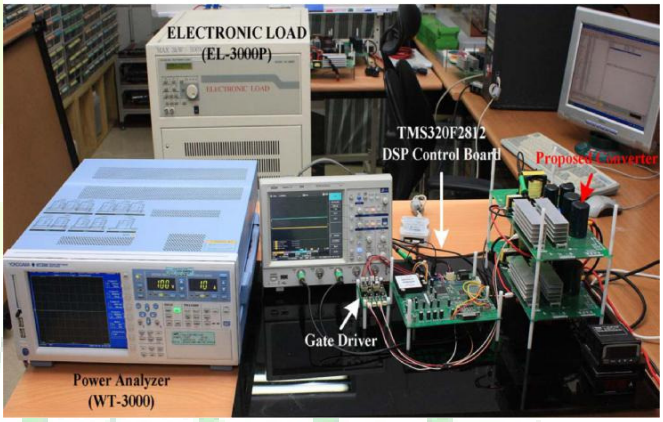

Fig. 8. Experimental setup.

V. EXPERIMENTAL RESULTS

Experiments were performed on a 1.2-kW prototype in order to verify the analysis and simulation results. The experimental parameter is given in Table I, used in the experimental system and specifications are given in Table II.

Control scheme of the proposed converter topology consists of current balance control and MPPT control. Fig. 9 shows the control block diagram. The maximum power point (MPP) voltage is calculated by the MPPT (i.e., P&O MPPT) using

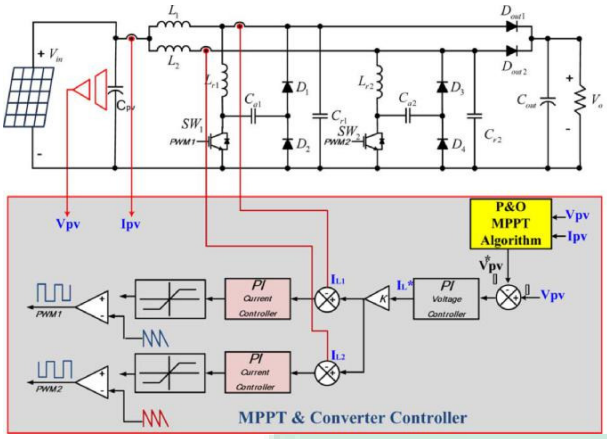

Fig. 9. Control algorism of proposed topology

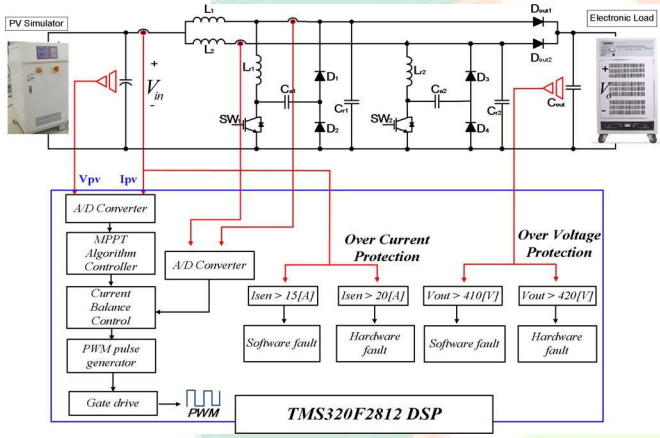

Fig. 10. Block diagram of experimental setup.

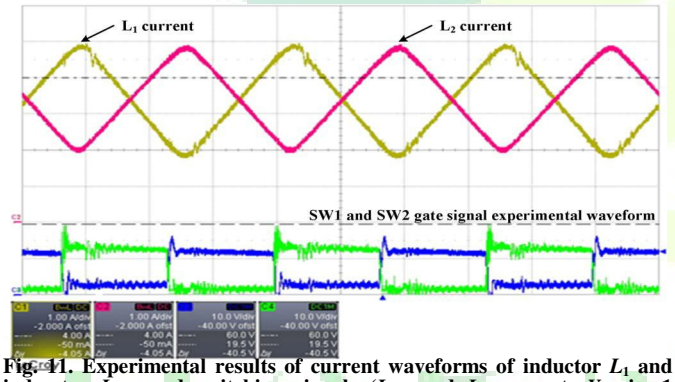

Fig. 11. Experimental results of current waveforms of inductor L_1 and induc-tor L_2 , and switching signals (L_1 and L_2 current; *Y*-axis: 1 A/division, gate signal; *Y*-axis: 10 V/division, *X*-axis: 10 μs/division).

detected PV voltage and current [20]. Calculated MPP voltage is compared with the detected PV voltage. The difference between the calculated MPP voltage and detected PV voltage is used as an input of voltage controller (i.e., the first PI controller). The output of the voltage controller is used as a current reference. The current reference is divided by the number of phase. Divided current reference is compared with the current of each phase, and the difference is used as an input of current controller. The gate signal is generated by comparison between the carrier

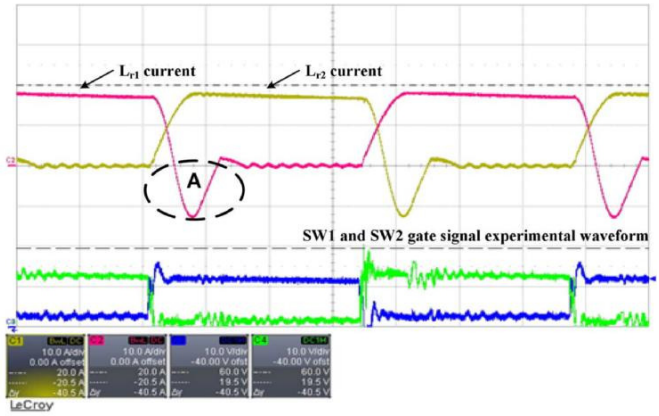

Fig. 12. Experimental results of the resonant inductor $L_{r\ 1}$ and $L_{r\ 2}$ current and switching signals ($L_{r\ 1}$ and $L_{r\ 2}$ current; *Y*-axis: 1 A/division, gate signal; *Y*-axis: 10 V/division, *X*-axis: 5 μs/division).

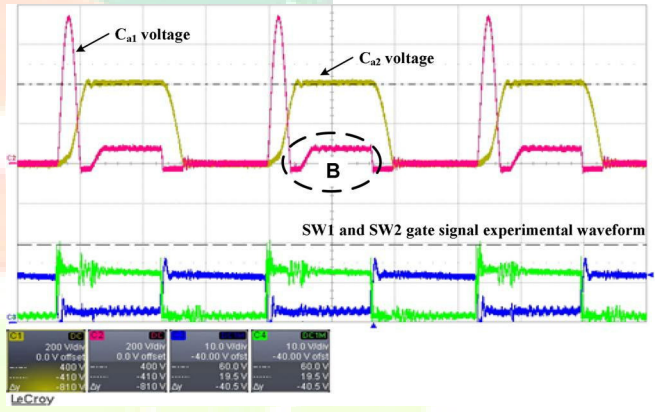

Fig. 13. Experimental results of voltage waveforms of $C_{a\ 1}$, $C_{r\ 1}$, and switch-ing signals ($C_{a\ 1}$ and $C_{a\ 2}$ voltage; *Y*-axis: 200 V/division, gate signal; *Y*-axis: 10 V/division, *X*-axis: 10 μs/division).

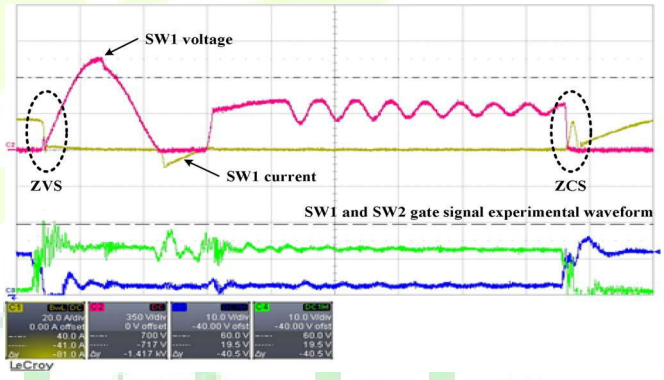

Fig. 14. Experimental results of the current and voltage of switching devices and switching signals (SW1 voltage; *Y*-axis: 350 V/division, SW1 current; *Y*-axis: 20 A/division, gate signal; *Y*-axis: 10 V/division, *X*-axis: 2 μs/division).

signal and the output of the current controller. From this, it can be confirmed that the phase difference between the gate signals of each phase is equal to 180° because there are two phases in the proposed interleaved soft-switching boost converter.

Fig. 8 shows the experimental setup of proposed converter (see Fig. 9).

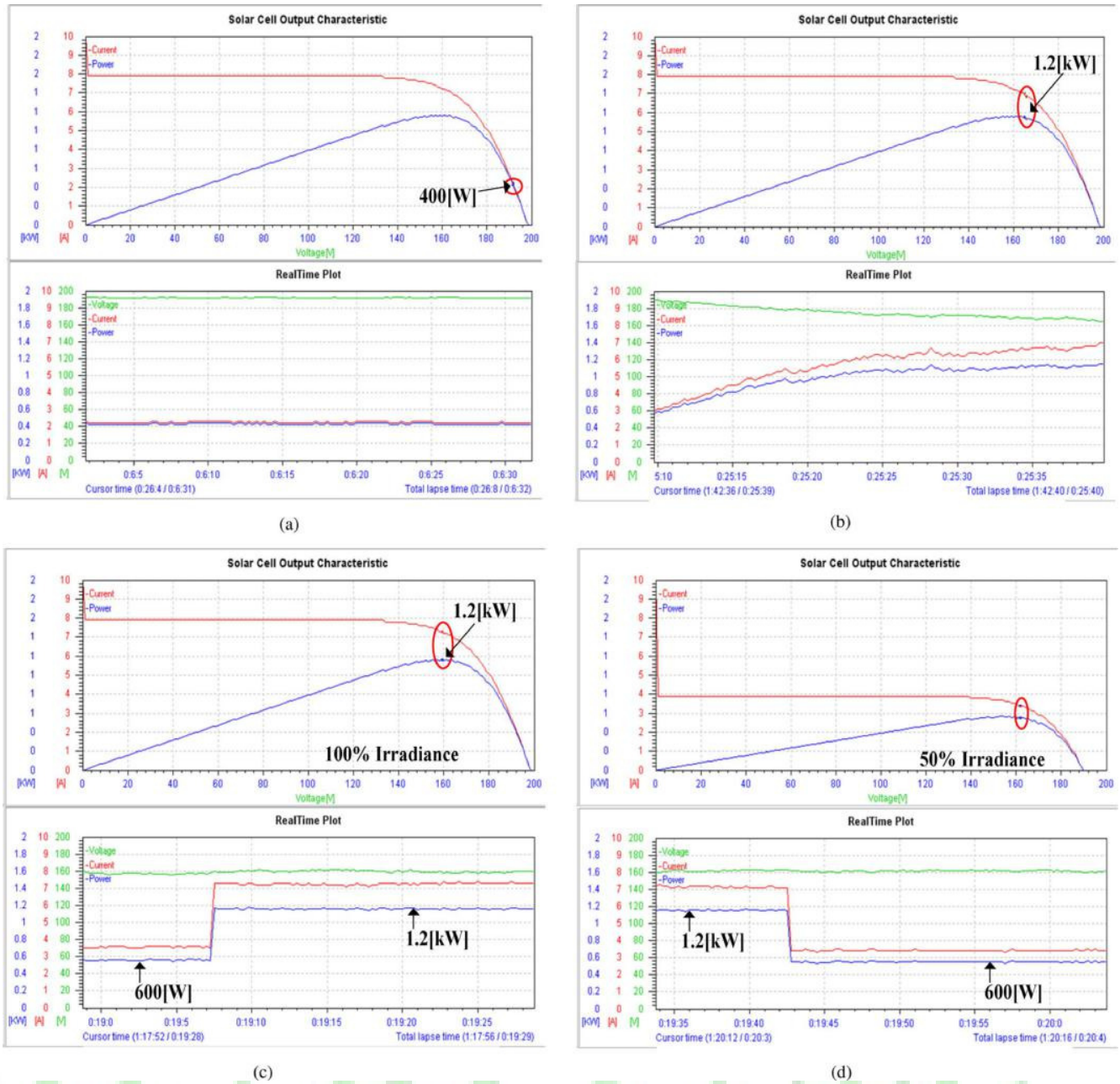

Fig. 15. Experimental MPPT results of the proposed ISSBC. (a) Non MPPT operation. (b) MPPT operation. (c) Irradiance 50% → 100%. (d) Irradiance 100% → 50%.

Fig. 10 depicts the block diagram of the proposed ISSBC for the MPPT test. The PV simulator condition used in the test was assumed to consist of the short current 8 A, open volt-age 200 V and maximum power 1.2 kW. The system control was implemented in DSP *TMS320F2812*. The output voltage and current were detected in the ISSBC for MPPT control and current balancing control.

Fig. 11 represents the current of the main inductor L_1 and L_2 , and gate signals (SW1 and SW2) under a full load. As the input current is the sum of the inductor currents, the input current ripple is almost zero. The experimental results obtained from the prototype are very similar to those shown in Fig. 5.

Fig. 12 shows the current waveforms of the resonant inductor $L_{r\,1}$, $L_{r\,2}$, and gate signals. The current through $L_{r\,1}$ and $L_{r\,2}$ are more than twice the main inductor L_1 and L_2 current, and it should drop below zero in area A.

Fig. 13 shows the voltage waveforms of the resonant capacitor and auxiliary resonant capacitor, and gate signals (SW1 and SW2). Compared with the simulation result in Fig. 6, there is a charging voltage of $C_{a\,1}$ shown in area B of Fig. 13. The difference was caused by the output capacitance of the switch (FGA25N120FRD).

Fig. 14 shows the experimental results of the switches volt-age and current, and gate signals. As expected from the mode

TABLE III
EFFICIENCY OF THE PROPOSED ISSBC TOPOLOGY

Load	Switching	Pi (*W*)	Po (*W*)	Effi. (*η*)
10%	Hard	142.01	120	84.5
	Soft	141.17	120	85.0
20%	Hard	265.69	240	90.33
	Soft	264.22	240	90.83
30%	Hard	383.79	360	93.8
	Soft	381.76	360	94.3
40%	Hard	507.39	480	94.6
	Soft	504.73	480	95.1
50%	Hard	631.84	600	94.96
	Soft	625.26	600	95.96
60%	Hard	754.32	720	95.45
	Soft	746.5	720	96.45
70%	Hard	876.09	840	95.88
	Soft	867.05	840	96.88
80%	Hard	1000.52	960	95.95
	Soft	988.16	960	97.15
90%	Hard	1125.23	1080	95.98
	Soft	1111.33	1080	97.18
100%	Hard	1255.49	1200	95.58
	Soft	1233.55	1200	97.28

analysis, the ZCS or ZVS operations of the switches show good performance.

Fig. 15 shows the experimental MPPT results of the proposed ISSBC. Fig. 15(a) shows the current, voltage, and power wave-forms of the PV simulator without MPPT control. The power point of the PV simulator operates near the open voltage and the PV simulator provides 400 W, which corresponds to 30% of maximum power.

Fig. 15(b)–(d) shows the current, voltage, and power wave-forms of the PV simulator with MPPT control. As seen in the *I–V* and *P–V* curves of Fig. 15(b), the proposed system operates at the maximum power point. Compared with Fig. 15(a), the voltage decreases and the current increases from 2*A* to 7*A*, and thus, the PV simulator provides 1200 W.

Fig. 15(c) shows the MPPT results; the irradiance changes from 50% to 100%. Fig. 15(d) shows the MPPT results; the irradiance changes from 100% to 50%. As seen in Fig. 15(c) and (d), MPPT control show good performance under the irradiance change.

Table III shows results of efficiency comparison between proposed soft-switching interleaved boost converter and con-ventional interleaved boost converter. In this comparison, same switching devices are applied to each converter prototypes.

VI. CONCLUSION

In this paper, we proposed a soft-switching interleaved boost converter using resonance. Numerical-mode analysis was per-formed for the design of the proposed ISSBC. From this anal-ysis, an example of an optimal design for resonant components was represented. To verify the feasibility of the proposed ISSBC, a 1.2-kW prototype was implemented.

In the experiment, MPPT control was performed by using a PV simulator, and current balancing control was performed. From the experimental results, it was confirmed that the resonant components are well designed. The efficiency of the proposed ISSBC was measured under the load variation condition and efficiency is measured by the power analyzer *WT 3000*.

The proposed converter is compared with the conventional in-terleaved hard switching boost converter under the same switch-ing frequency and power conditions.

For the conventional interleaved hard switching boost con-verter and proposed ISSBC, the total efficiencies are measured for various load currents, as shown in Table III.

REFERENCES

[1] J.-P. Lee, B.-D. Min, T.-J. Kim, D.-W. Yoo, and J.-Y. Yoo, "Design and con-trol of novel topology for photovoltaic dc/dc converter with high efficiency under wide load ranges," *J. Power Electron.*, vol. 9, no. 2, pp. 300–307, Mar. 2009.

[2] B.-D. Min, J.-P. Lee, and J.-H. Kim, "A novel grid-connected PV PCS with new high efficiency converter," *J. Power Electron.*, vol. 8, no. 4, pp.309–316, Oct. 2008.

[3] G. Hua, C.-S. Leu, Y. Jiang, and F. C. Y. Lee, "Novel zero-voltage-transition PWM converters," *IEEE Trans. Power Electron.*, vol. 9, no. 2, pp.213–219, Mar. 1994.

[4] G. Hua, E. X. Yang, Y. Jiang, and F. C. Y. Lee, "Novel zero-current-transition PWM converters," *IEEE Trans. Power Electron.*, vol. 9, no. 6, pp.601–606, Nov. 1994.

[5] H. Bodur and A. F. Bakan, "A new ZVT-ZCT-PWM DC-DC converter," *IEEE Trans. Power Electron.*, vol. 19, no. 3, pp. 676–684, May 2004.

[6] H. Bodur and A. F. Bakan, "A new ZVT-PWM DC-DC converter," *IEEE Trans. Power Electron.*, vol. 17, no. 1, pp. 40–47, Jan. 2002.

[7] N. Jain, P. K. Jain, and G. Joos, "A zero voltage transition boost con-verter employing a soft switching auxiliary circuit with reduced conduc-tion losses," *IEEE Trans. Power Electron.*, vol. 19, no. 1, pp. 130–139, Jan. 2004.

[8] S. K. Kwon and K. F. A. Sayed, "Boost-half bridge single power stage PWM DC-DC converters for PEM-fuel cell stacks," *J. Power Electron.*, vol. 8, no. 3, pp. 239–247, Jul. 2008.

[9] X. Kong and A. M. Khambadkone, "Analysis and implementation of a high efficiency, interleaved current—Fed full bridge converter for fuel cell system," *IEEE Trans. Power Electron.*, vol. 22, no. 2, pp. 543–550, Mar. 2007.

[10] H. M. Suryawanshi, M. R. Ramteke, K. L. Thakre, and V. B. Borghate, "Unity-power-factor operation of three-phase ac–dc soft switched con-verter based on boost active clamp topology in modular approach," *IEEE Trans. Power Electron.*, vol. 23, no. 1, pp. 229–236, Jan. 2008.

[11] H. Mao, O. Abdel Rahman, and I. Batarseh, "Zero-voltage-switching dc– dc converters with synchronous rectifiers," *IEEE Trans. Power Electron.*, vol. 23, no. 1, pp. 369–378, Jan. 2008.

[12] H. Tao, A. Kotsopoulos, J. L. Duarte, and M. A. M. Hendrix, "Transformer-coupled multiport ZVS bidirectional dc–dc converter with wide input range," *IEEE Trans. Power Electron.*, vol. 2, pp. 771–781, Mar. 2008.

[13] H. Xiao and S. Xie, "A ZVS bidirectional dc–dc converter with phase-shift plus PWM control scheme," *IEEE Trans. Power Electron.*, vol. 23, no. 2, pp.813–823, Mar. 2008.

[14] D. V. Ghodke, K. Chatterjee, and B. G. Fernandes, "Three-Phase three level, soft switched, phase shifted PWM dc–dc converter for high power applications," *IEEE Trans. Power Electron.*, vol. 23, no. 3, pp. 1214–1227, May 2008.

[15] M. Borage, S. Tiwari, S. Bhardwaj, and S. Kotaiah, "A full-bridge dc–dc converter with zero-voltage-switching over the entire conversion range," *IEEE Trans. Power Electron.*, vol. 23, no. 4, pp. 1743–1750, Jul. 2008.
[16] S. Y. Tseng, J. Z. Shiang, H. H. Chang, W. S. Jwo, and C. T. Hsieh, "A novel turn-on/off snubber for interleaved boost converter," *Proc. IEEE 38th Annu. Power Electron. Specialists Conf. (PESC 2007)*, 2718–2724.
[17] X. Wu, J. Zhang, X. Ye, and Z. Qian, "Analysis and derivations for a family ZVS converter based on a new active clamp ZVS cell," *IEEE Trans. Ind. Electron.*, vol. 55, no. 2, pp. 773–781, Feb. 2008.
[18] P.-W. Lee, Y.-S. Lee, D. K. W. Cheng, and X.-C. Liu, "Steady-state analysis of an interleaved boost converter with coupled inductors," *IEEE Trans. Ind. Electron.*, vol. 47, no. 4, Aug. 2000.
[19] D.-Y. Jung, Y.-H. Ji, J.-H. Kim, C.-Y. Won, and Y.-C. Jung, "Soft switching boost converter for photovoltaic power generation system," *Proc. 13th*

